

Phospholipid-Free Small Unilamellar Vesicles for Drug Targeting to Cells in the Liver

Wunan Zhang, Roland Böttger, Zhu Qin, Jayesh A. Kulkarni, Julian Vogler, Pieter R. Cullis, and Shyh-Dar Li*

It is reported that cholesterol (Chol) and TWEEN 80 at a molar ratio of 5:1 can form small unilamellar vesicles (SUVs) using a staggered herringbone micromixer. These phospholipid-free SUVs (PFSUVs) can be actively loaded with a model drug for targeting hepatocytes via the endogenous apolipoprotein mechanism. PFSUVs particles with compositions of Chol:TWEEN 80 ranging between 1.5:1 and 5:1 (mol/mol) can be produced with a mean diameter of ≈80 nm, but only the high-Chol formulations (3:1 and 5:1) can retain a transmembrane gradient of ammonium sulfate for active loading of doxorubicin (DOX). Under cryo-transmission electron microscopy, PFSUVs-DOX displays a unilamellar bilayer structure with DOX molecules forming spindle-shape aggregates inside the aqueous core. Relative to PEGylated liposomal doxorubicin (PLD) that exhibits little interaction with cells in various conditions, the cellular uptake of PFSUVs-DOX is dependent on the presence of serum and enhanced with an increased concentration of apolipoproteins. After intravenous injection, the vast majority of PFSUVs-DOX accumulates in the liver and DOX is detected in all liver cells (predominantly the hepatocytes), while PLD is captured only by the sinusoidal cells (i.e., macrophages). This report discloses an innovative lipid bilayer vesicle for highly efficient and selective hepatocyte targeting.

1. Introduction

Lipid vesicles with a bilayer structure have been utilized extensively for drug delivery. [1,2] Fifteen phospholipid-based formulations have already succeeded in clinical trials since the approval of Doxil in 1995 and significantly motivated the development of related delivery systems. [3] Several nonphospholipid materials have been reported to construct similar bilayer structures with differential properties extending the scope of applications. [4,5] Surfactants, most often supplemented with cholesterol

W. Zhang, Dr. R. Böttger, Dr. Z. Qin, J. Vogler, Prof. S.-D. Li Faculty of Pharmaceutical Sciences University of British Columbia Vancouver, British Columbia V6T 1Z3, Canada E-mail: shyh-dar.li@ubc.ca Dr. J. A. Kulkarni, Prof. P. R. Cullis Department of Biochemistry and Molecular Biology University of British Columbia Vancouver, British Columbia V6T 1Z3, Canada

The ORCID identification number(s) for the author(s) of this article can be found under https://doi.org/10.1002/smll.201901782.

DOI: 10.1002/smll.201901782

(Chol), can form bilayer vesicles known as niosomes.[5,6] Niosomal formulations are capable of encapsulating hydrophilic and hydrophobic drugs in the aqueous core and the lipophilic membrane, respectively.[7-10] Niosomes have been extensively used in the cosmetic industry and studied for topical drug delivery for decades.[11-13] However, intravenous (i.v.) administration of niosomes is investigated much less frequently.[14,15] Niosomal formulations given i.v. only displayed marginal differentiation in pharmacokinetics (PK) compared with free drugs and are therefore regarded as inadequate for systemic delivery. [15,16] These studies investigated the use of surfactants in combination with a minor to equimolar content of Chol. It was shown that once the surfactant content increased above 50 mol%, the resulting lipid membrane could no longer hold a barrier to prevent burst drug leakage in physiological environments, which in turn diminished their ability to modify the PK and biodistribution (BD) of drugs.[17-19]

Additionally, relatively high surfactant ratios in the membrane (>50 mol%) resulted in increased ion permeability, which hampered the formation of a transmembrane gradient required for active drug loading.^[20] For the past decades, ≈50 mol% has been widely assumed as the maximum Chol content possible to be incorporated in all types of lipid bilayer vesicles.^[21,22] A number of studies concluded that an equimolar content of surfactant and Chol is the optimal formulation for niosomes regarding stability and pharmaceutical properties. Again, these highin-surfactant formulations surfered from nonoptimal stability for systemic drug delivery.^[23–26] Increasing the Chol content could augment membrane rigidity to reduce the membrane permeability and drug leakage. Nevertheless, the audacious attempts of fabricating a formulation with an increased Chol ratio higher than 50 mol% have failed in the past decade.^[24,27]

Niosomes are mostly prepared with the thin-film hydration method, sometimes followed by membrane extrusion to control the size homogeneity. This method has not been successful to prepare niosomal formulations containing >50 mol% Chol. Novel manufacturing strategies are to be investigated for producing diverse formulations. Recently, microfluidics was utilized to produce conventional niosomes; however, it was not possible to incorporate a Chol content higher than equimolar



with this technique either.^[7,9,29–31] In this study, we utilized a staggered herringbone micromixer (SHM) to engineer nanosized vesicles with a high Chol content (>50 mol%). Chol was first dissolved in ethanol with a surfactant, TWEEN 80, and this organic phase collided with an aqueous phase within the SHM system, allowing self-assembly of Chol and TWEEN 80 into a bilayer structure in a controlled manner. Here, we report the development and optimization of the Chol:TWEEN 80 formulation and the microfluidic conditions for fabricating high-Chol phospholipid-free small unilamellar vesicles (PFSUVs) for active loading of a weak-base model drug, doxorubicin (DOX). We then compared the drug release profile, PK, and BD of PFSUVs-DOX with the standard PEGylated liposomal doxorubicin (PLD). The drug targeting mechanism of PFSUVs-DOX was also investigated. To the best of our knowledge, this work was the first successful attempt to fabricate PFSUVs with a high Chol content capable for active loading of an ionizable drug and demonstration of its unique in vivo PK and BD for hepatocyte targeting.

2. Results and Discussion

2.1. Fabrication of Empty PFSUVs

PFSUVs with different Chol/TWEEN 80 ratios were fabricated using the SHM. Briefly, TWEEN 80 and Chol were dissolved in ethanol and infused into a microfluidic chip alongside with an ammonium sulfate (AS) solution. As the lipid solution got diluted with water leading to increased polarity, Chol and TWEEN 80 self-assembled into particles. These particles were collected and transferred into a tangential flow filtration (TFF) system, which removed ethanol, exchanged the exterior buffer to create an AS gradient for active drug loading, and concentrated the formulations (Figure 1). PFSUV particles with Chol/TWEEN 80 ratios of 1.5:1, 2:1, 3:1, and 5:1 (mol/mol, referred

to as PFSUVs 1.5:1, 2:1, 3:1, and 5:1, respectively) showed a similar mean diameter around 70 nm (Figure 2A). The particle size remained constant under storage at 4 °C for at least 10 d without any precipitates, indicating good stability. In contrast, PFSUVs 8:1 showed an increased diameter of 115 nm, and upon storage at 4 °C, the size continued to increase and was therefore not suitable for drug delivery applications. The increase of particle size could result from the aggregation of Chol molecules that could no longer be homogeneously dispersed by TWEEN 80 molecules due to their large content (88 mol%). PFSUVs 5:1 corresponding to a molar Chol content of 83% was found to be the upper Chol limit to form stable particles using SHM, and the cryo-transmission electron microscopy (cryo-TEM) showed that PFSUVs 5:1 displayed a small unilamellar vesicular structure (Figure 2B). During the microfluidic process, rapid mixing of the lipid solution with the aqueous phase resulted in a rapid increase in the polarity of the medium. The solution quickly achieved a state of high supersaturation of both TWEEN 80 and Chol monomers throughout the entire mixing volume followed by rapid and homogeneous nucleation of the lipids, which in turn initiated the self-assembly of lipid nanoparticles. The rapid nucleation event could occur within 1 ms for ultrafast nanoparticle formation before the concentration of Chol exceeded the limit of aggregation.^[32] This unique process allowed successful fabrication of PFSUVs containing up to 83 mol% Chol.

2.2. Optimization of Active Drug Loading Conditions

Active loading offers several advantages compared to passive loading, including increased loading efficiency and enhanced drug association with the particles without rapid drug leakage. DOX was used as a model drug in the whole study, as its active loading method has been well established with a clinically approved product Doxil (Johnson & Johnson), and DOX is a fluorescent molecule that can be easily detected and imaged. PFSUVs were

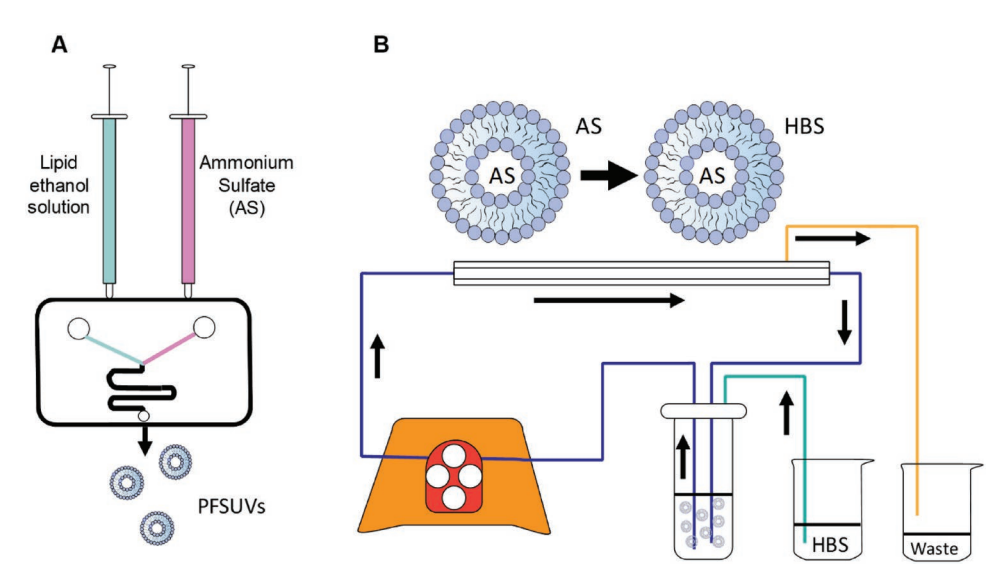


Figure 1. Schematic illustration of PFSUVs preparation. A) Chol and TWEEN 80 dissolved in ethanol were mixed with AS in a SHM to produce PFSUVs. B) The exterior phase of the particles was then exchanged with HBS (pH = 7.4) to achieve a transmembrane gradient using TFF.

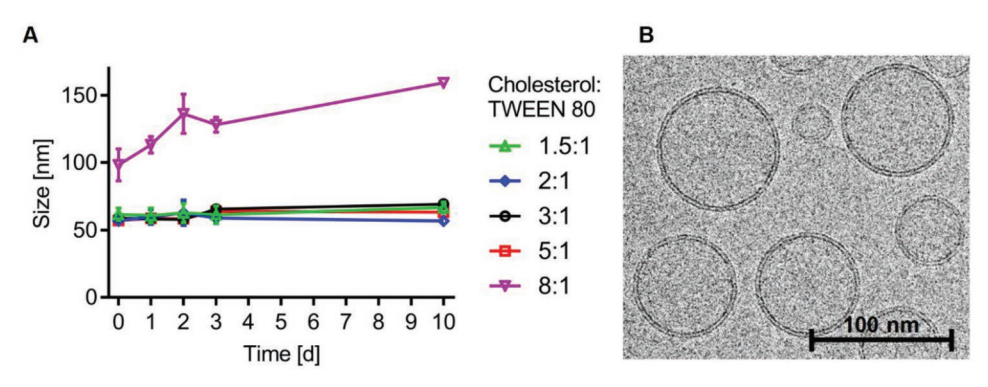


Figure 2. A) Stability of empty PFSUVs with different ratios of Chol/TWEEN 80 stored at 4 °C in HBS. The particle size was monitored for 10 d using a particle analyzer. B) Cryo-TEM images of PFSUVs 5:1 indicated the formation of a small unilamellar vesicular structure.

first fabricated in 120×10^{-3} M AS, followed by TFF to remove ethanol and exchange the exterior buffer to 4-(2-hydroxyethyl)-1-piperazineethanesulfonic acid buffered saline (HBS, pH 7.4) to create a transmembrane gradient (inner core: AS; exterior: HBS). The PFSUVs were then incubated with DOX at different drug-to-lipid ratios at various temperatures for different periods of time. After the drug loading, particle size and drug encapsulation efficiency (EE) of formulations prepared under different conditions were compared. At loading temperatures of 20 and 37 °C, the size of the final particles remained at 55–75 nm for all tested formulations (**Figure 3A**). After incubation at 45 °C, PFSUVs 1.5:1 increased its size to 145 nm, while PFSUVs 2:1,

3:1, and 5:1 remained at their initial size of 60–80 nm. When the loading temperature was further increased to 60 °C, all PFSUV formulations displayed an increased size to 100–175 nm. This temperature-induced particle aggregation of PFSUVs was dependent on the formulation. Formulations that contained an increased amount of TWEEN 80 tended to aggregate upon incubation at elevated temperatures. Particles with a TWEEN 80 content above 33%, i.e., PFSUVs 1.5:1 and 2:1, could not actively load DOX under all tested conditions (Figure 3B). High TWEEN 80 formulations might not contain a stable bilayer structure to maintain the transmembrane gradient for active drug loading. Only the formulations with a high Chol ratio (3:1 and 5:1, mol/mol)

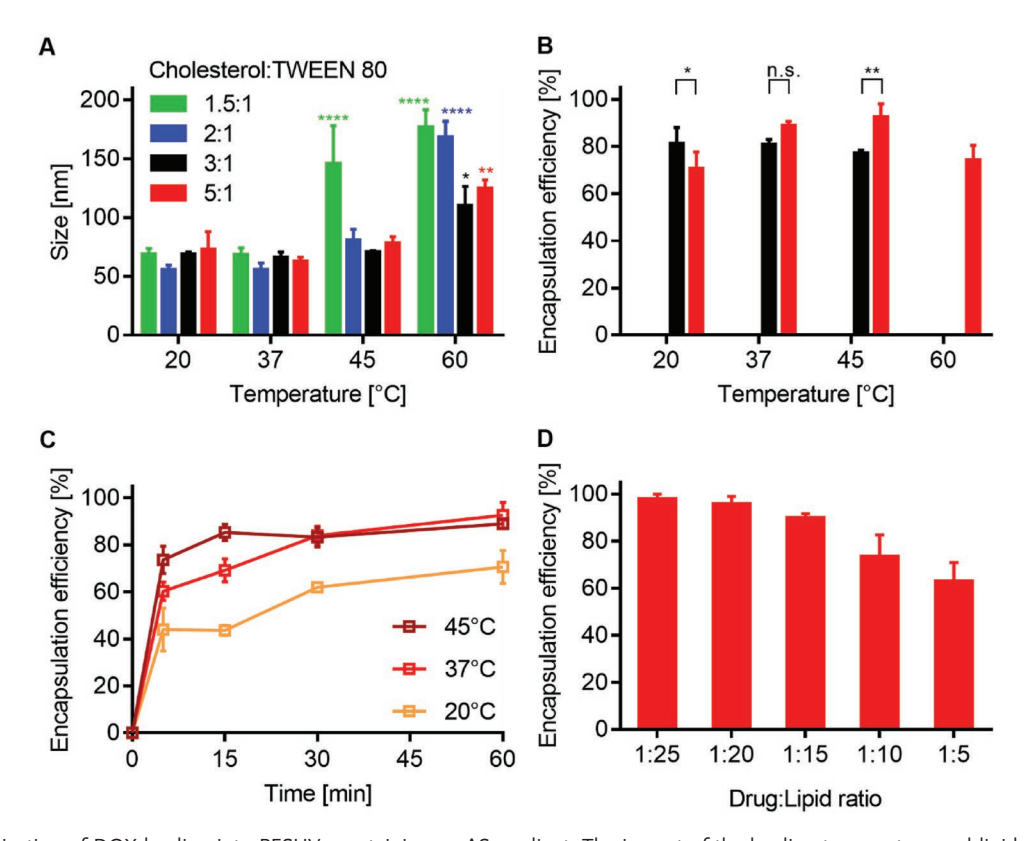


Figure 3. Optimization of DOX loading into PFSUVs containing an AS gradient. The impact of the loading temperature and lipid composition was investigated by monitoring A) the particle size and B) encapsulation efficiency (EE). C) The loading kinetics into PFSUVs 5:1 was measured at different temperatures. D) Furthermore, the D/L ratio was optimized. Data points represent mean \pm SD (n = 3).

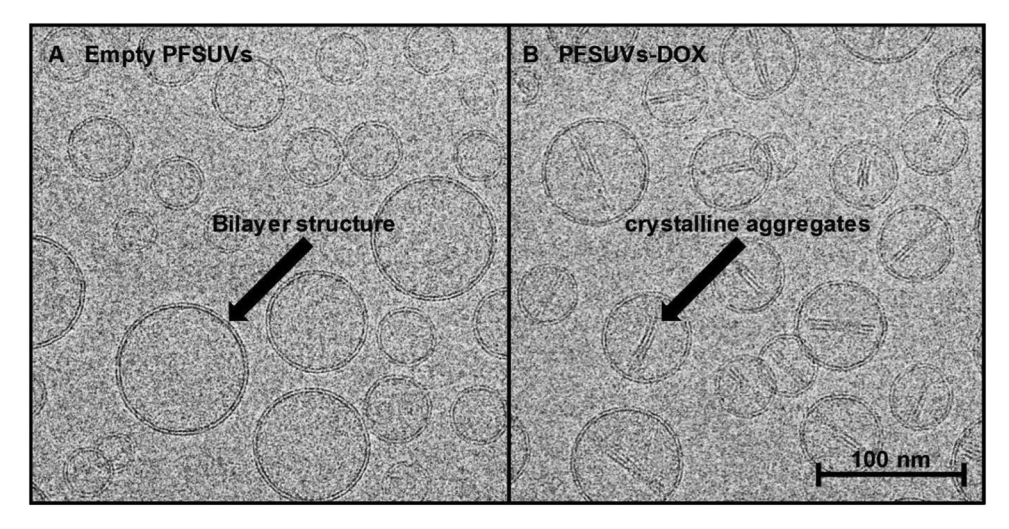


Figure 4. A) Cryo-TEM images of empty PFSUVs indicating a bilayer structure and B) DOX-loaded PFSUVs showing crystalline aggregates inside the core.

could successfully load DOX via the AS gradient. For PFSUVs 3:1, the EE performed at 20 to 45 °C was comparable at ≈80%, while at 60 °C no drug was loaded. On the other hand, the EE for PFSUVs 5:1 displayed an increasing trend from 71% to 93% with increasing temperature from 25 to 45 °C. However, at 60 °C, the EE of PFSUVs 5:1 decreased to 75%. The results suggest that Chol stabilized the bilayer at high temperatures but also decreased the membrane permeability for DOX permeation. Therefore, to promote drug loading into PFSUVs with a high Chol content, the loading temperature needed to be increased to enhance the membrane permeability. However, an excessive increase of the loading temperature destabilized the bilayer, inducing particle aggregation and reducing the drug loading efficiency. Based on these results, we selected the PFSUVs 5:1 formulation for further studies, as it displayed the highest stability and drug loading efficiency. Furthermore, this formulation contains the least amount of TWEEN 80 with fewer concerns about surfactant-induced side effects such as hemolysis.[33] Indeed, this formulation did not induce hemolysis of sheep red blood cells (Figure S1, Supporting Information) at a wide range of concentrations.

We then examined the drug loading kinetics with PFSUVs 5:1 (referred to as PFSUVs from now on) at 20–45 °C. As shown in Figure 3C, increasing the incubation temperature facilitated drug loading. EE reached the maximum of 60% in 30 min for 20 °C incubation, 80% in 30 min for 37 °C, and 82% in 15 min for 45 °C, respectively, at a drug/lipid ratio (D/L) of 1/10 (w/w). We then fixed the loading temperature at 37 °C and studied the EE at a range of D/L. As shown in Figure 3D, EE of >95% could be achieved at a D/L of 1:20 (w/w). The EE decreased with increasing D/L, indicating the EE reached its maximum at the D/L of 1:20. We then selected these conditions to prepare

PFSUVs-DOX for the following studies. We first compared the structures of empty PFSUVs and PFSUVs-DOX using cryo-TEM. As shown in Figure 4, PFSUVs exhibited a morphology of small unilamellar vesicle with a bilayer structure, and DOXloaded PFSUVs contained a needle-like object in the aqueous core, which was also reported with Doxil.[34] This spindlelike object is anticipated to be the insoluble crystalline of DOX-sulfate formed after active loading.[35] Unlike Doxil, whose morphology is altered from a spherical shape to the olive shape due to the growth of the spindle aggregates inside the liposome, the morphology of PFSUVs-DOX remained as spherical. It is noted that besides the AS gradient, the citric acid gradient was also employed to actively load DOX into PFSUVs with comparable results (Figures S2 and S3, Supporting Information). This indicates significant potential of PFSUVs for maintaining various transmembrane gradients for loading of different drugs.

2.3. Comparison between PLD and PFSUVs-DOX

To the best of our knowledge, this is the first report of successful fabrication of small unilamellar vesicles prepared without a phospholipid but only a surfactant TWEEN 80 and >50 mol% of Chol. This report also demonstrates that a drug could be actively loaded into this type of vesicles. We then characterized PFSUVs-DOX with various in vitro and in vivo assays and compared this innovative delivery system with a reference formulation, PLD. We first prepared PLD following the protocols and compared the key physicochemical properties between PFSUVs-DOX and PLD (Table 1).^[36] PFSUVs-DOX (76 nm) prepared by microfluidics were smaller than PLD (111 nm)

Table 1. Physical properties of PFSUVs-DOX and PLD. Data = mean \pm SD (n = 3).

Formulation	Composition	Method	D/L ratio	EE [%]	Drug loading value [w%]	Size [nm]	PDI	ZP [mV]
PFSUVs-DOX	Tween 80/Chol (1/5)	Microfluidics	1:20	96 ± 3	4.8 ± 0.2	76.5 ± 4.5	0.132 ± 0.027	-5.5 ± 3.5
PLD	DSPC/DSPE-mPEG2000/ Chol (38/4/25)	Thin-film hydration	1:8	95 ± 1	11.9 ± 0.2	111.3 ± 9.7	0.036 ± 0.003	-24.7 ± 1.9

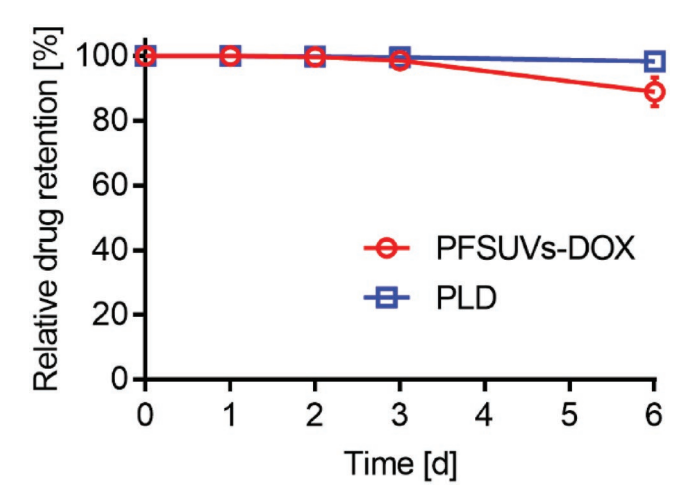


Figure 5. In vitro drug retention of PFSUVs-DOX and PLD in 50% FBS at 37 °C. Data = mean \pm SD (n = 3).

fabricated by the thin-film hydration method. The polydispersity index (PDI) of PFSUVs-DOX (0.132 \pm 0.027) was higher than PLD (0.036 \pm 0.003), but in an acceptable range (<0.2). The particle size variation within each formulation was low, indicating that both PFSUVs-DOX and PLD were highly reproducible. The zeta potentials (ZPs) of PFSUVs-DOX and PLD were -5 and -25 mV, respectively. The negative surface charge of PLD was due to the phosphate groups of N-(carbonylmethoxypolyethylene glycol 2000)-distearoyl-glycerophosphoethanolamine (DSPE-PEG2000) in the formulation. PLD provided an increased D/L compared to PFSUVs-DOX (1:8 vs 1:20, w/w), indicating a higher drug content per PLD particle, while both formulations exhibited similar EE (≈95%). The drug loading value of drug per PFSUVs and PLD weight was 4.8 weight% (w%) and 11.9 w%, respectively. We then compared PFSUVs-DOX and PLD in various in vitro and in vivo assays.

2.4. Drug Retention

Both PLD and PFSUVs-DOX stably retained DOX when incubated with 50% fetal bovine serum (FBS) for at least 6 d, demonstrating <10% drug leakage (Figure 5). In previous studies, 50%–80% of drug leakage from niosomal formulations was reported after 24–48 h incubation.^[15,16] To the best of our knowledge, this is the first report showing that a drug could be stably retained in a surfactant-based SUV formulation. It has been demonstrated that nanoparticles having weak association with drugs provide no enhancements in improving pharmacokinetics and drug targeting.^[37]

2.5. Pharmacokinetics and Biodistribution

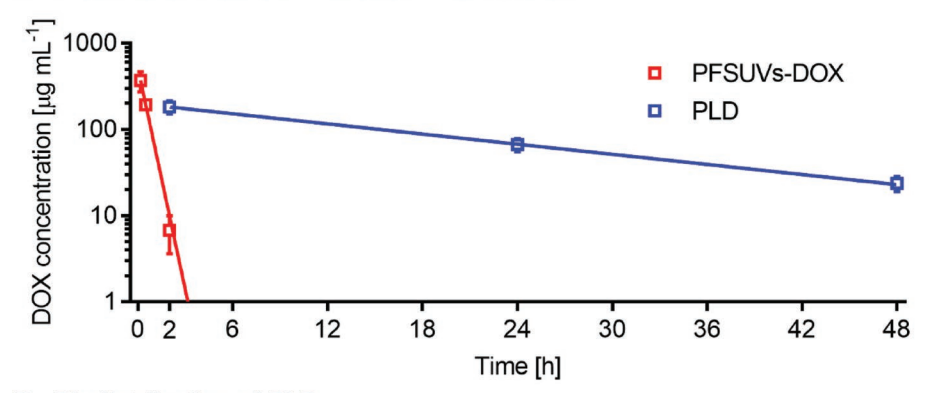
The improved serum stability of PFSUVs-DOX allowed us to study the PK and BD of this innovative delivery system in comparison with PLD. PFSUVs-DOX or PLD were i.v. injected into BALB/C mice at a dose of 5 mg DOX kg⁻¹. After 10 min, 0.5, 2, 24, and 48 h (PFSUVs-DOX) or 2, 24, and 48 h (PLD) plasma and various tissues were collected for DOX measurement. As

shown in **Figure 6**A, PLD displayed prolonged blood circulation and a significant plasma concentration of PLD (23.7 μ g mL⁻¹) was still detected 2 d post injection, while PFSUVs-DOX was rapidly removed from the plasma by 2 h. The PK data were analyzed by the noncompartmental model using the PKSolver software to obtain and compare key PK parameters, including half-life ($t_{1/2}$), volume of distribution (V_2), clearance (CL), and area under the curve (AUC) (**Table 2**). The data show that PFSUVs-DOX displayed 52-fold decreased $t_{1/2}$, 3-fold reduced V_z , 18-fold increased CL, and 18-fold decreased AUC compared to PLD. The PK of our PLD was consistent with the literature. [36] The PK of PFSUVs-DOX differed significantly from that of PLD, suggesting a unique biodistribution profile.

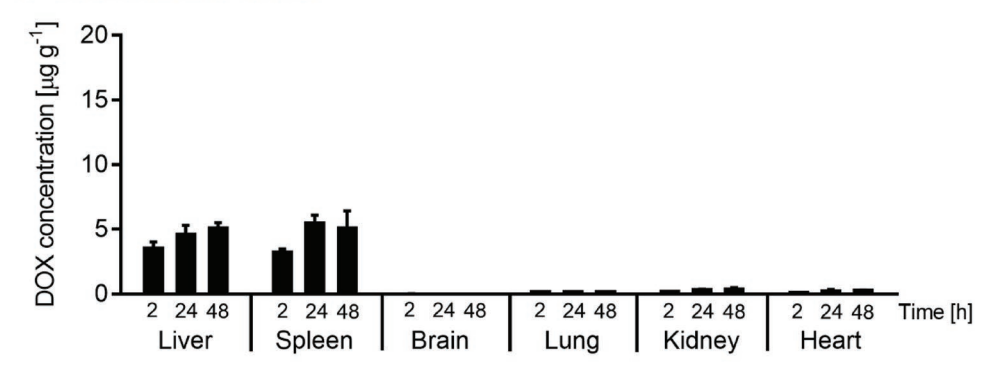
We therefore compared the tissue distribution of the two formulations. As shown in Figure 6B, PLD was mainly taken up by the liver and spleen (3–5 μg g⁻¹ tissue) with minimal concentrations detected in other tissues (<0.3 µg g⁻¹ tissue), including the brain, lungs, kidneys, and heart. It is also noted that the spleen and liver uptake of PLD occurred as soon as 2 h with 3-4 µg g⁻¹ and gradually increased over time to 5 μ g g⁻¹ in 1–2 d. In comparison with the plasma data, the tissue uptake levels of PLD were minimal, indicating the majority of PLD remained in the blood circulation. The results with PLD are consistent with the literature. [38,39] On the other hand, within 2 h after injection, PFSUVs-DOX was largely detected in the liver with a concentration of $15 \mu g g^{-1}$, which explains the rapid plasma clearance, but the liver concentrations rapidly declined to $<1 \mu g g^{-1}$ in 1 d (Figure 6C). The spleen clearance of PFSUVs-DOX was also significant relative to other tissues that only showed low uptake ($<1 \mu g g^{-1}$), including the brain, lungs, kidneys, and heart. However, the spleen uptake of PFSUVs-DOX was only moderate $(2-3 \mu g g^{-1})$ compared to the liver. The data indicate that PFSUVs-DOX rapidly distributed to the liver after i.v. administration, leaving low concentrations in the plasma and other tissues. Additionally, this BD profile is different compared to free DOX, which is predominantly found in the kidney 1 h post i.v. injection with minimal uptake by the liver, as shown by us in a previous report.^[40] Therefore, we conclude that PFSUVs provided liver targeting.

The BD profiles of PFSUVs-DOX were distinctive from PLD. In particular, the liver uptake of PLD increased over time, while that for PFSUVs-DOX declined rapidly after 2 h, suggesting different mechanisms. The liver is composed of different cell types, mainly the hepatocytes (60% of total liver cells) and macrophages (Kupffer cells, 10%–15% of total liver cells). [41,42] A variety of nanoparticles have been shown to be recognized by the Kupffer cells for plasma clearance, including PLD. [43] We then compared the intraliver uptake profiles of PLD and PFSUVs-DOX. Figure 7A shows the confocal images of the liver sections collected 2 h after injection of PLD or PFSUVs-DOX. Fluorescein-phalloidin was used to label cellular actins to differentiate the hepatocytes from the sinusoidal cells (mostly Kupffer cells). PFSUVs effectively delivered DOX to all the cells in the liver, while PLD was almost exclusively associated with sinusoidal cells. The quantitative results show that on average there were 217 hepatocytes and 91 sinusoidal cells per field of the liver section image and >90% were positive with DOX, after treatment with PFSUVs-DOX (Figure 7A,C). The data indicate that PFSUVs were effective in delivering DOX to various cell types in the liver, and the hepatocytes accounted for the major uptake. In contrast, only 2%

A Pharmacokinetics of PLD and PFSUVs-DOX



B Biodistribution of PLD



C Biodistribution of PFSUVs-DOX

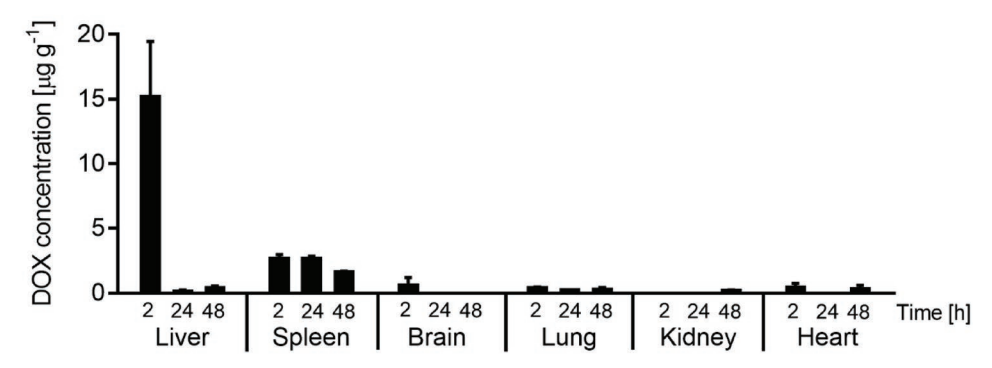


Figure 6. A) Semi-log plot of plasma concentrations and B,C) biodistribution of PLD and PFSUVs-DOX after intravenous administration at 5 mg DOX kg⁻¹ in BALB/C mice. Data = mean \pm SD (n = 3-5).

of the hepatocytes were associated with PLD, which was predominantly delivered to sinusoidal cells (16%). To further demonstrate PFSUVs targeted cells in the liver, we labeled PFSUVs with a lipophilic dye 1,1'-dioctadecyl-3,3,3',3'-tetramethylindotricarbocyanine iodide (DiR) that would not penetrate cell membranes in its free form and found that the fluorescence signals after i.v. administration of PFSUVs-DiR were detected in the cytoplasm of liver cells (Figure S4, Supporting Information).

Consistent with the biodistribution data (Figure 6C,D), the overall uptake of PFSUVs-DOX by the liver was higher than PLD, but interestingly, PFSUVs-DOX declined rapidly after 2 h (Figure 6D). A similarly rapid removal of PFSUVs-DOX was also demonstrated in the brain, but not other tissues. Both hepatocytes and blood-brain barrier have been shown to express

a variety of drug efflux pumps, such as P-glycoprotein that has been shown to remove DOX. [44] PLD was not effectively removed by the liver because the delivery was focused to the Kupffer cells, rather than the hepatocytes (Figure 7). It has to be noted that these efflux phenomena are most likely specific for DOX, which was utilized as a model drug in this study, and results may be different for other drugs this delivery system may be applied to.

2.6. Cellular Uptake and Liver Targeting Mechanism

TWEEN 80 incorporated in nanoparticles has been shown to mediate adsorption of apolipoproteins. [45,46] Additionally, PFSUVs contain a high concentration of Chol, which may

Table 2. Pharmacokinetic parameters of PFSUVs-DOX and PLD after i.v. injection in mice determined with PKSolver software using a noncompartmental model. Parameters include elimination half-life $(t_{1/2})$, volume of distribution during terminal phase (V_z) , area under the plasma concentration—time curve from time zero to infinity $(AUC_{0-\infty})$, and total body clearance of the drug from plasma (CL).

Formulation	PFSUVs-DOX	PLD	
Dose [mg kg ⁻¹]	5	5	
t _{1/2} [h]	0.3	15.6	
$V_{\rm z} [{\rm mL~kg^{-1}}]$	9.1	25.3	
$CL [mL kg^{-1} h^{-1}]$	20.0	1.1	
$AUC_{0-\infty}$ [µg mL ⁻¹ h]	250.2	4448.9	

harness the endogenous Chol uptake mechanism by the liver, again through the apolipoproteins.^[47] Apolipoprotein coating is a well-known uptake mechanism for several lipid nanoparticle formulations,^[48–53] because apolipoproteins are a known ligand for the low-density lipoprotein (LDL) receptor family expressed by the hepatocytes, including the LDL receptor, LDL receptor-related protein, very low-density LDL receptor, and ApoE receptor 2.^[53] Among these receptors, the LDL receptor was demonstrated to be the major

contributor responsible for internalization of a polipoprotein-coated nanoparticles. $\sp(48)$

To test the proposed involvement of apolipoproteins, we compared the cellular uptake of PLD and PFSUVs-DOX by LDL receptor positive cells in the presence and absence of serum or apolipoproteins. As shown in Figure 8 while free DOX penetrated into the cells and bound with the nuclear DNA effectively in all the tested conditions, there was no cellular internalization of PLD under any conditions. It has been shown that PEGylated particles exhibit minimal interaction with cell membrane due to the steric hindrance.^[54] On the other hand, PFSUVs were taken up by all cells in the presence of serum, suggesting serum components were critical for the uptake. Furthermore, the PFSUVs-DOX signal increased over increasing concentrations of apolipoproteins in the medium. Thus, the data support our hypothesis of apolipoprotein dependency of the cellular uptake, which could be most likely attributed to the LDL receptors expressed on the cell surface.

Since receptors of the LDL receptor family are overexpressed by cells in the liver including the hepatocytes and Kupffer cells, the mechanisms for the liver-targeted delivery of PFSUVs are hypothesized as follows: (a) Upon i.v. administration, the serum apolipoproteins rapidly adsorb onto PFSUVs; (b) As the liver is a highly perfused organ with high hepatic blood flow (0.95 mL min⁻¹ in BALB/C mice), [55] a large amount

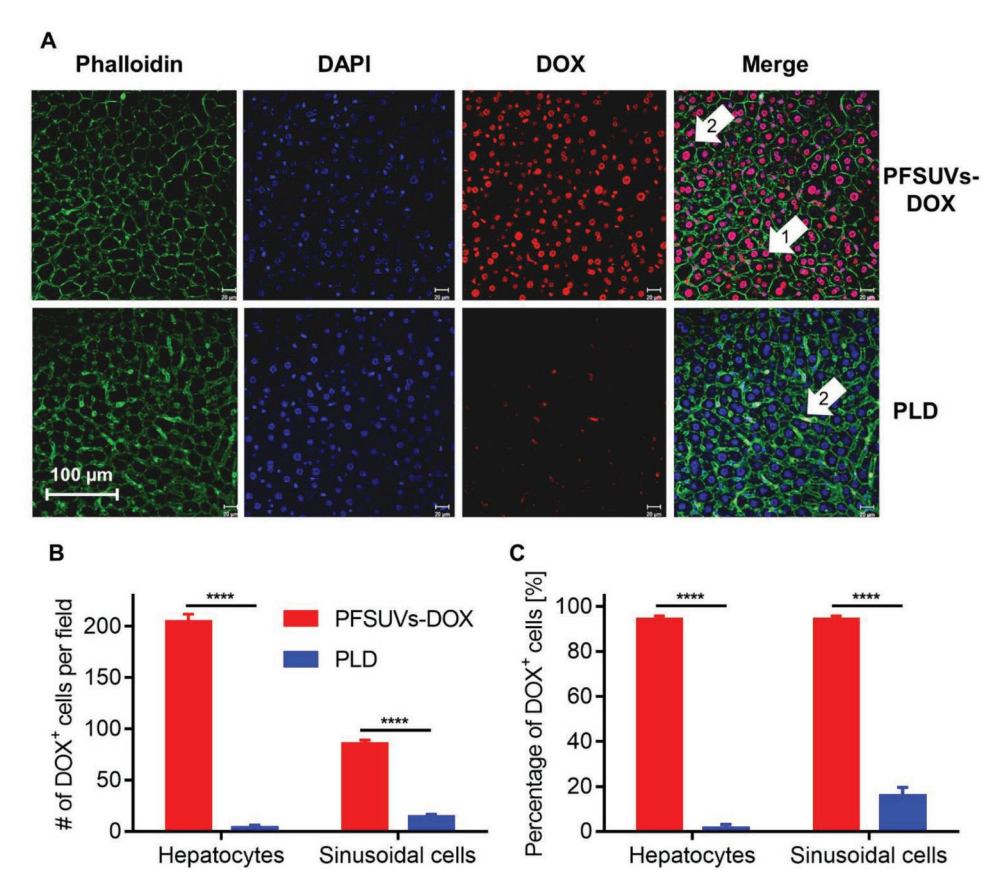


Figure 7. A) Confocal microscopy images of liver sections taken from mice 2 h after intravenous treatment with PFSUVs-DOX or PLD at 5 mg DOX kg $^{-1}$. Nuclei were stained with DAPI (blue), cytoskeletons were stained with fluorescein-phalloidin (green), and DOX was visualized in red. Arrows 1 and 2 indicate hepatocellular and sinusoidal (Kupffer cell) uptake of DOX, respectively. B) Total number of DOX-positive hepatocytes and sinusoidal cells per microscopy images (n = 3) and C) corresponding percentage of DOX-positive of each cell type.

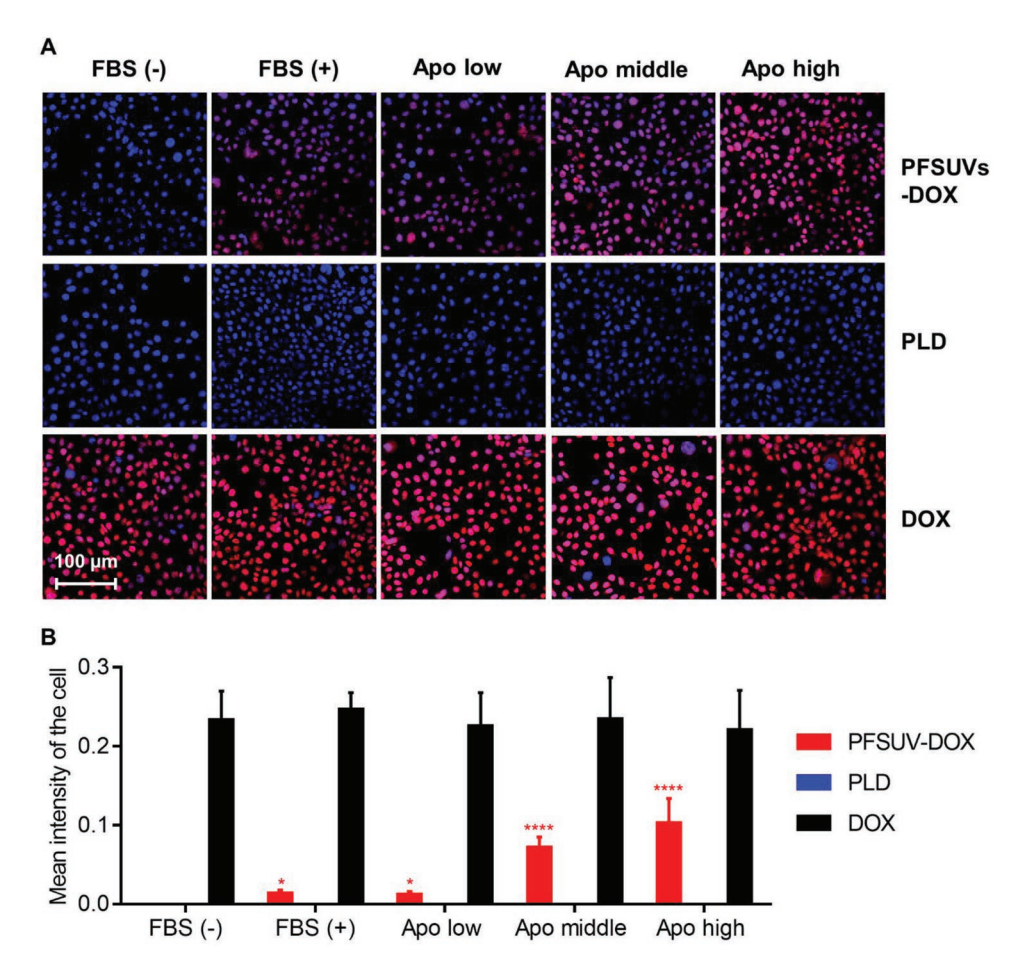


Figure 8. The uptake of PFSUVs-DOX and PLD by LDL receptor positive EMT-6 cells under different conditions. A) Confocal images of cells after 4 h incubation and B) quantitative results measured by the CellProfiler software. Data = mean \pm SD (n = 100 cells). Apo low, middle, and high represent concentrations of apolipoproteins in the culture medium at 5, 20, and 100 μ g mL⁻¹, respectively.

of apolipoprotein-coated PFSUVs-DOX would reach the liver within a short time. That way the liver would be preferred over organs also containing LDL receptor positive cells, but showing slower blood flow, such as the lungs (0.25 mL min⁻¹) and brain (0.39 mL min⁻¹); (c) A fraction of PFSUVs (size ≈80 nm) was captured by the Kupffer cells in the sinusoid, while the rest penetrated through the sinusoidal fenestrae (≈100 nm) due to the small size and interacted with the hepatocytes^[56,57]; (d) Apolipoprotein-coated PFSUVs were recognized possibly through the binding with receptors of the LDL receptor family expressed by all cells in the liver, including the hepatocytes, Kupffer cells, and hepatic stellate cells, for internalization.^[58] As a result, all the cells in the liver were positive with DOX via the delivery of PFSUVs (Figure 7). We summarized the hypothesized mechanism in Figure 9.

2.7. Potential Future Applications of PFSUVs

Liver diseases are a global health problem accounting for ≈2 million deaths per year worldwide, including liver cirrhosis, hepatitis B, and hepatocellular carcinoma. [59,60] Both sinusoidal cells and hepatocytes are crucially involved in these diseases.

Current nanoparticle delivery technologies mainly target Kupffer cells that represent 10%–15% of the liver cells. [41,42] A drug delivery system that also targets other types of liver cells, including the hepatocytes, the dominant liver cells (≈60%), will be highly desirable for improving therapy of liver diseases. Additionally, PFSUVs can maintain transmembrane gradients for active loading of drugs, making this formulation attractive for targeting a wide range of therapeutic agents to treat various liver disorders. To show that PFSUVs will be potentially useful for the treatment of major liver diseases, we encapsulated several drugs relevant for liver diseases at the same conditions as optimized for DOX (Table 3).

Malaria is characterized with an initial liver stage, where parasite sporozoites invade hepatocytes and undergo asexual replication before progressing to the blood. [61] Quinone drugs are used to treat malaria and efficient liver targeting to stop malaria progression at the liver stage remains a challenge. [62] We encapsulated the weakly basic quinine drug chloroquine using the AS gradient into PFSUVs achieving an EE of 95.4%. Further development of this delivery system encapsulated with chloroquine and other quinine-based drugs such as primaquine could be highly beneficial for liver-stage malaria treatment. [63] Another liver-related infectious disease related to liver impairment is

Figure 9. Schematic illustration of the hypothesized liver-targeting mechanism of PFSUVs-DOX in a sinusoid capillary. After binding with apolipoproteins in the plasma upon i.v. administration, PFSUVs-DOX was recognized by the Kupffer cells attached to the endothelium via the LDL receptor. PFSUVs-DOX can also penetrate the hepatic sinusoidal fenestrae and interact with hepatocytes via the LDL receptor family.

viral hepatitis (hepatitis B and hepatitis C) resulting in liver cirrhosis and hepatocellular carcinoma.^[64] Immune modulators targeting the Toll-like receptor 7/8 such as imiquimod and resiguimod (R848) have been investigated as an interferonalpha booster to treat hepatitis C.[65,66] Both imiquimod and R848 are weakly basic drugs and could be efficiently loaded into PFSUVs (EE: 98.2% and 93.3%, respectively) using the AS gradient. Finally, liver injury induced by a variety of agents such as alcohol, environmental pollutants, dietary components, and drugs, resulting in progression of steatohepatitis, liver fibrosis, or cirrhosis remains a problem in society.[59,60] Curcumin, a natural product isolated from turmeric, exerts hepatoprotective and therapeutic effects on several liver diseases associated with oxidative stress and inflammation through various cellular and molecular mechanisms.^[67] Nanoformulations of curcumin are an emerging field for improving the bioavailability and organ targeting of this compound. [68] As a hydrophobic drug, we encapsulated curcumin in the bilayer of PFSUVs via passive loading (EE = 88.9% at a D/L of 1/40). Potential in medical applications of these formulations will be demonstrated in future studies.

3. Conclusion

For the first time, we have shown that a PFSUV containing 83 mol% Chol and 17 mol% TWEEN 80 could be fabricated using a staggered herringbone micromixer with a mean diameter of 76.5 nm. Due to the high Chol content, the bilayer was stable to maintain a transmembrane gradient for active loading of a weak-base model drug DOX. This is also the first example that PFSUVs could stably retain a drug and improve the drug

targeting after systemic delivery. PFSUVs-DOX displayed unique PK and BD profiles compared to PLD. In particular, we demonstrated that after i.v. administration, PFSUVs rapidly accumulated in the liver and delivered DOX to all the cells in the liver, including hepatocytes (vast majority), while PLD was only found within the sinusoidal cells (i.e., Kupffer cells).

4. Experimental Section

Preparation of PFSUVs: PFSUVs with optimized Chol/TWEEN 80 (Sigma-Aldrich, Oakville, ON, Canada) molar ratios (5:1) were prepared in a controlled nanoprecipitation process using a two-channel microfluidic system (NanoAssemblr Benchtop, Precision Nanosystems International, Vancouver, BC, Canada). The NanoAssemblr was equipped with a microfluidic cartridge that contained the SHM design (dimensions $6.6 \times 5.5 \times 0.8$ cm, Precision Nanosystems International). Solutions were injected into the cartridge via polypropylene syringes (Becton, Dickinson and Company, Franklin Lakes, NJ) with a size of 10 and 3 mL for aqueous and organic phases, respectively. Chol and TWEEN 80 were dissolved in ethanol (Greenfield Global, Toronto, ON, Canada) at a final concentration of 10 mg mL⁻¹ and mixed with 120 mmol L⁻ aqueous AS solution (Sigma-Aldrich) in the microfluidic system at a flow ratio of 1/3 between ethanol and the aqueous phase. Alternatively, AS was replaced by 300 mmol L⁻¹ citric acid (Sigma-Aldrich). Per run, 12 mL of particle suspension was produced at a total flow rate of 15 mL min⁻¹ and the procedure was conducted at room temperature. Raw PFSUVs (50 mL) were then subjected to a TFF system (KrosFlo KR2i, Spectrum Laboratories, Rancho Dominguez, CA) to remove ethanol, exchange the exterior phase to HBS (pH 7.4) or 100 mmol L⁻¹ sodium acetate buffer (pH 5, Sigma Aldrich), and concentrate. In the TFF system operating in the ultrafiltration mode, PFSUVs were filtered through a diafiltration cartridge with a molecular weight cut-off of 500 kDa (MidiKros Hollow Fiber Filter, surface area 115 cm², fiber inner diameter 0.5 mm, length 20 cm, Spectrum Laboratories) at a flow rate of

Table 3. Physical properties of PFSUVs loaded with different drugs. Data = mean \pm SD (n = 3).

Formulation	Loading method	D/L ratio	EE [%]	Drug loading value [w%]	Size [nm]	PDI
PFSUVs-chloroquine	Active loading	1:20	95.4 ± 2.2	4.8 ± 0.1	57.0 ± 0.4	0.13 ± 0.01
PFSUVs-imiquimod	Active loading	1:20	98.2 ± 4.7	4.9 ± 0.3	57.5 ± 3.4	0.13 ± 0.03
PFSUVs-R848	Active loading	1:20	93.3 ± 8.1	4.7 ± 0.5	50.1 ± 0.8	0.09 ± 0.02
PFSUVs-curcumin	Passive loading	1:40	88.9 ± 8.6	2.2 ± 0.2	56.4 ± 0.6	$\textbf{0.10} \pm \textbf{0.04}$

140 mL min⁻¹ and concentrated to 30 mg mL⁻¹ total lipid concentration. Chol concentration in PFSUVs after diafiltration and concentration was determined using a Chol E assay kit (FUJIFILM Wako Diagnostics Corporation, Richmond, VA). The average particle size was measured using dynamic light scattering (Zetasizer NanoZS, Malvern Instruments, Malvern, UK). Error bars represent three average size measurements of the same formulation. The short-term storage stability of empty PFSUVs was evaluated by storage in HBS at 4 °C. At selected time points (0, 1, 2, 3, and 10 d), the size of PFSUVs was measured.

Drug Loading: PFSUVs (2.0 mg total lipids) were incubated with 100 µg drug in the appropriate buffer (final volume 1 mL). DOX (Alomone Labs, Jerusalem, Israel) and chloroquine diphosphate (Sigma-Aldrich) were loaded in HBS (pH 7.4), whereas imiquimod and R848 (both Cayman Chemical, Ann Arbor, MI, USA) were loaded in 100 mmol L⁻¹ sodium acetate buffer (pH 5). The mixture was incubated for 1 h at 37 °C and then quenched on ice for 2 min. The drug-loaded particles were subjected to purification by TFF as described above in the diafiltration mode using ten diafiltration volumes of buffer.

The EE of DOX was calculated using UV–vis spectroscopy as described earlier with some modifications. [69] Briefly, PFSUVs-DOX in HBS (10 μ L) was mixed with NaOH (2 μ L, 4 mol L⁻¹) and HBS (2 μ L) and transferred immediately to a spectrophotometer (NanoDrop 2000, Thermo Fisher Scientific, Burnaby, BC, Canada) to detect the absorbance at 600 nm. The final EE was calculated using Equation (1), where R_s represents the sample absorbance, R_0 represents the absorbance of a mixture containing PFSUVs-DOX (10 μ L) and HBS (4 μ L), and R_{100} represents the absorbance of PFSUVs-DOX (10 μ L) mixed with NaOH (2 μ L, 4 mol L⁻¹) and aqueous Triton-X 100 (2 μ L, 10%, w/w, Thermo Fisher Scientific)

$$EE = 1 - \frac{R_s - R_0}{R_{100} - R_0} \tag{1}$$

The encapsulated contents of chloroquine, imiquimod, and R848 were determined using ultra performance liquid chromatography (UPLC). PFSUVs (20 µL) were lysed by adding 40 µL methanol (VWR, Mississauga, ON, Canada) and sonication (5 min). Samples were analyzed on an ACQUITY UPLC H-Class System (Waters, Milford, MA) coupled online to a photodiode array detector. Separation relied on a BEH-C18 column (inner diameter: 2.1 mm; length: 50 mm; particle size: 1.7 μm , Waters; column temperature: 60 °C) at a flow rate of 0.3 mL min⁻¹ using a linear aqueous methanol gradient in the presence of trifluoroacetic acid (TFA, ≈98%, Alfa Aesar, Tewksbury, MA). Eluent A and B consisted of 0.1% v/v aqueous TFA and methanol containing 0.1% v/v TFA, respectively, and were mixed in the following gradient. 1 min: A/B (95/5); 6 min: A/B (0/100); 3 min: A/B (0/100); 1 min: A/B (95/5); 2 min: 1 min: A/B (95/5). Drugs and cholesterol were detected via absorbance at 342 nm (chloroquine), 320 nm (imiquimod and R848), and 205 nm (cholesterol), respectively, and quantified using calibration curves to calculate drug loading values. The encapsulation efficiency was calculated as a ratio of drug loading values before and after purification of the freshly loaded particles.

Alternatively, curcumin (Alfa Aesar) was encapsulated into PFSUVs at a D/L of 1/40 via a passive loading approach during their preparation. Chol, TWEEN 80, and curcumin at a molar ratio of 72.5:25:25:25 were dissolved in ethanol at a final concentration of 10 mg mL $^{-1}$. This solution was mixed with PBS in the microfluidic system at a flow ratio of 1/3 between ethanol and the aqueous phase. The setting of the microfluidic preparation process and purification was as described above. The encapsulation efficiency of curcumin-loaded particles was determined using UPLC as described above with detection of curcumin at an absorbance of 430 nm.

Cryo-TEM: The morphology of empty PFSUVs and PFSUVs-DOX was imaged by Cryo-TEM (FEI Titan Krios, Hillsboro, OR) following a previously described method. [70] Sample preparation was performed using the Mark IV Vitrobot (FEI, Hillsboro, OR) at the UBC Bioimaging Facility. About 2–4 μ L of PFSUVs and PFSUVs-DOX at 25 mg lipid mL $^{-1}$ was applied to a copper grid and plunge-frozen in liquid ethane to generate vitreous ice. The frozen samples were stored in liquid nitrogen

until imaging. The FEI Titan Krios (Hillsboro, OR) at the Life Sciences Institute (UBC) was operated at 300 kV under low-dose conditions with images collected on a Falcon 3 (FEI) direct electron detector. A nominal underfocus of 0.5–1.5 µm was used to enhance image contrast.

Preparation and Characterization of PLD: The thin-film hydration method was utilized to prepare PLD as described before with some modifications. [36] Briefly, 1,2-distearoyl-sn-glycero-3-phosphocholine (DSPC)/Chol/DSPE-PEG2000 (32 mg, 38:25:4, mol/mol/mol, Avanti Polar Lipids, Alabaster, AL) was dissolved in chloroform (Thermo Fisher Scientific). The organic solvent was removed under vacuum (BÜCHI Labortechnik AG, Flawil, Switzerland) at 60 °C. The thin-film was hydrated with 250 mmol L⁻¹ AS at 60 °C for 45 min and sonicated for 10 min (ultrasonic bath, Thermo Fisher Scientific). The lipid suspension was extruded for ten times through 100 nm and then 50 nm Nucleopore Track-Etch membranes (Sigma-Aldrich RTC, Laramie, WY) using a mini-extruder (Avanti Polar Lipids). Liposomes were dialyzed against HBS (pH 7.4, 1:1000, v/v) overnight. The final lipid concentration of liposomes was determined by the Chol E kits.

DOX (1 mg) was mixed with empty liposomes (8 mg total lipid) in a total volume of HBS (1 mL). The loading mixture was incubated at 60 °C for 45 min and then quenched in ice for 2 min. Free DOX was removed by dialysis against HBS for 8 h (1: 1000, v/v). PLD was subsequently filtered through a 0.22 μm polyethersulfone membrane (Thermo Fisher Scientific) for sterilization. PLD was characterized for its size, PDI, and ZP by a particle analyzer (Zetasizer). The DOX concentration and EE were measured using the same method as described for PFSUVs.

In Vitro Drug Retention: DOX leakage from particles was investigated using a previously described method with minor modifications. [71] PLD and PFSUVs-DOX were diluted with sterile PBS to adjust the DOX concentration to 50 μg mL $^{-1}$, then mixed 1:1 with FBS (Gibco Laboratories, Gaithersburg, MD), and incubated at 37 °C. After 1, 2, 3, and 6 d, the sample (10 μL) was collected and diluted 30-fold with PBS. The sample (225 μL) was transferred to a 96-well plate, PBS (25 μL) was added, and the fluorescence was detected using a microplate reader (excitation: 485 nm; emission: 590 nm; Hidex, Turku, Finland). The relative drug retention at each time point was calculated using Equation (2), where F_t denotes the fluorescence at the selected time point, F_0 is the fluorescence at time 0, and F_{100} is the fluorescence of a mixture containing diluted sample (225 μL) and aqueous Triton-X 100 (25 μL , 10%, w/w), followed by incubation at room temperature in the dark for 15 min

Relative drug retention =
$$\left(1 - \frac{F_t - F_0}{F_{100} - F_0}\right) * 100\%$$
 (2)

Pharmacokinetics and Biodistribution Study: Female BALB/C mice (18–20 g, 6–7 weeks old) were purchased from The Jackson Laboratory (Bar Harbor, ME). All the in vivo studies were conducted in accordance with the established experimental protocols (ID: A18-0177) approved by the Animal Care Committee of the University of British Columbia (Vancouver, BC, Canada).

PFSUVs-DOX or PLD was administered to mice via the tailvein injection at 5 mg DOX kg^{-1} . At 2, 24, and 48 h, the plasma was isolated and DOX concentration was measured using a previously reported method.^[40] After euthanasia, the heart, liver, spleen, kidneys, lungs, and brain were excised. The tissues were washed twice with PBS, blotted dry, and weighted into a 1.5 mL microtube (Next Advance, Inc., Troy, NY). Typically, tissue (0.1-0.3 g) was collected, a nuclear lysis buffer (0.3 mL per 0.1 g organ) containing 10 mmol L⁻¹ HEPES, 1 mmol L⁻¹ MgSO4, and 1 mmol L⁻¹ CaCl₂ in water (pH 7.4) was added, and tissue homogenization was performed with a tissue homogenizer Precellys 24 (Bertin Technologies, Courtland, CA). The homogenate (100 µL) was transferred into a 1.5 mL microtube, and aqueous Triton X-100 (50 $\mu L,~10\%,~w/w),~water~(100~\mu L),~and$ acidified isopropanol (750 μ L, 0.75 mol L⁻¹ HCl) were added and the mixture was stored at -20 °C overnight. After thawing, the mixture was equilibrated to room temperature for 1 h, centrifuged (10 min, 12 000 \times g), and the supernatant (250 μ L) was loaded onto a 96-well plate for DOX quantification by fluorescence spectroscopy by comparing the fluorescence intensity with a calibration curve generated by spiking



known amounts of DOX into different tissue homogenates of untreated mice. Pharmacokinetic data sets were evaluated with a PKSolver add-in for Microsoft Excel using noncompartmental analysis.^[72]

Microscopic Liver Analysis: The livers from PFSUVs-DOX and PLD treated mice were harvested 2 h post injection, fixed in aqueous formaldehyde (10%, v/v), and sectioned using a vibratome (Precisionary Instruments, Boston, MA). Tissue sections with a thickness of 40 μ m were collected in PBS and soaked inside 1% Triton-X 100 (w/w) solution for 15 min. Fluorescein-phalloidin (4 U mL⁻¹, Thermo Fisher Scientific) was applied to stain the tissue for 15 min at room temperature. After being washed with PBS for three times, the section was placed on a glass slide. One drop of Fluoroshield with 4',6-diamidino-2-phenylindole (DAPI) (Thermo Fisher Scientific) was applied on the section before it was sealed with a coverslip. The tissue section was then imaged by confocal microscopy.

Cellular Uptake: EMT-6 cells (LDL receptor positive) were cultured in Dulbecco's Modified Eagle Medium (Thermo Fisher Scientific) containing FBS (10%, v/v), penicillin (100 U mL⁻¹), and streptomycin (100 μg mL⁻¹) at 37 °C with 5% CO₂.^[73] EMT-6 cells were seeded on a coverslip and placed in a 24-well plate (10⁵ cells per well) for 24 h prior to the study. Cells were treated with DOX, PFSUVs-DOX, or PLD (5 μg DOX mL⁻¹) in the presence or absence of 10% FBS and a range of concentrations of human apolipoprotein (5, 20, and 100 μg mL⁻¹, BioVision Inc., Milpitas, CA) for 4 h. After removal of the medium, the cells were washed with PBS twice and fixed with 10% formaldehyde in PBS (Starplex Scientific, Etobicoke, ON) at room temperature for 20 min. The coverslip was washed twice with PBS and mounted on a glass slide with DAPI-Fluoroshield. The cells were imaged using a Zeiss confocal microscope (LSM 700, Carl Zeiss Canada, Toronto, ON, Canada) and the image was analyzed using the CellProfiler software (Version 3.0, Broad Institute, Cambridge, MA).

Statistical Analysis: All data are expressed as mean \pm standard deviation (SD). Statistical analysis was conducted with the two-tailed unpaired t-test for two-group comparison or one-way ANOVA (analysis of variance), followed by the Turkey multiple comparison tests (for three or more groups) by using GraphPad Prism software (GraphPad Software, San Diego, CA). A difference with p < 0.05 was considered to be statistically significant. (*: P < 0.05; **: P < 0.002; ****: P < 0.0001; n.s.: not significant.)

Supporting Information

Supporting Information is available from the Wiley Online Library or from the author.

Acknowledgements

W.Z. and R.B. contributed equally to this work. The Li lab was supported by grants from the Canadian Institutes of Health Research (CIHR; Grant No. PJT-148610), the Natural Science and Engineering Research Council in Canada (NSERC; Grant No. RGPIN-2017-03787), the Canada Foundation for Innovation (CFI; Grant No. 35816), and the Faculty of Pharmaceutical Sciences at the University of British Columbia (UBC). S.-D.L. received the CIHR New Investigator Salary Award and the Angiotech Professorship in Drug Delivery. The project was partially supported by a Mitacs Accelerate grant sponsored by Precision Nanosystems Inc. (Grant No. IT13402). This research project was supported in part by the High Resolution Macromolecular Cryo-Electron Microscopy facility at UBC. The authors like to thank Nojoud A. L. Fayez and K. K. Durga Rao Viswanadham for assistance with animal experiments, as well as Dominik Witzigmann, Johannes Lennart Bohrmann, and Alice Yu (all at UBC) for valuable discussions on the experimental designs.

Conflict of Interest

The authors declare no conflict of interest.

Keywords

drug delivery, liver targeting, microfluidics, phospholipid-free small unilamellar vesicles, staggered herringbone micromixer

Received: April 8, 2019 Revised: July 30, 2019 Published online: September 6, 2019

- [1] J. Qi, Y. Lu, D. Chen, L. Hovgaard, W. Wu, M. Cui, Int. J. Pharm. 2015, 489, 210.
- [2] S. Deshpande, Y. Caspi, A. E. C. Meijering, C. Dekker, *Nat. Commun.* 2016, 7, 10447.
- [3] U. Bulbake, S. Doppalapudi, N. Kommineni, W. Khan, *Pharmaceutics* 2017, 9, 12.
- [4] Z. K. Cui, T. Phoeung, P. A. Rousseau, G. Rydzek, Q. Zhang, C. Geraldine Bazuin, M. Lafleur, *Langmuir* 2014, 30, 10818.
- [5] S. Moghassemi, A. Hadjizadeh, J. Controlled Release 2014, 185, 22.
- [6] G. Amoabediny, F. Haghiralsadat, S. Naderinezhad, M. N. Helder, E. Akhoundi Kharanaghi, J. Mohammadnejad Arough, B. Zandieh-Doulabi, Int. J. Polym. Mater. Polym. Biomater. 2018, 67, 383.
- [7] S. Garcia-Salinas, E. Himawan, G. Mendoza, M. Arruebo, V. Sebastian, ACS Appl. Mater. Interfaces 2018, 10, 19197.
- [8] M. M. Ibrahim, T. M. Shehata, J. Drug Delivery Sci. Technol. 2018, 46, 14.
- [9] L. K. Yeo, T. O. B. Olusanya, C. S. Chaw, A. A. Elkordy, *Pharmaceutics* 2018, 10, 185.
- [10] N. Samed, V. Sharma, A. Sundaramurthy, Appl. Surf. Sci. 2018, 449, 567
- [11] R. M. Handjani-Vila, A. Ribier, B. Rondot, G. Vanlerberghie, Int. J. Cosmet. Sci. 1979, 1, 303.
- [12] H. Schreier, J. Bouwstra, J. Controlled Release 1994, 30, 1.
- [13] L. Abidin, M. Mujeeb, S. S. Imam, M. Aqil, D. Khurana, *Drug Delivery* 2016, 23, 1069.
- [14] I. F. Uchegbu, J. A. Double, J. A. Turton, A. T. Florence, *Pharm. Res.* 1995, 12, 1019.
- [15] A. Rogerson, J. Cummings, N. Willmott, A. T. Florence, J. Pharm. Pharmacol. 1988, 40, 337.
- [16] G. Parthasarathi, N. Udupa, P. Umadevi, G. Pillai, J. Drug Targeting 1994, 2, 173.
- [17] R. Muzzalupo, L. Pérez, A. Pinazo, L. Tavano, Int. J. Pharm. 2017, 529, 245.
- [18] L. Tavano, C. Oliviero Rossi, N. Picci, R. Muzzalupo, Int. J. Pharm. 2016, 511, 703.
- [19] S. K. Mehta, N. Jindal, AAPS PharmSciTech 2015, 16, 67.
- [20] R. Bartelds, M. H. Nematollahi, T. Pols, M. C. A. Stuart, A. Pardakhty, G. Asadikaram, B. Poolman, PLoS One 2018, 13, e0194179.
- [21] I. F. Uchegbu, A. T. Florence, Adv. Colloid Interface Sci. 1995, 58, 1.
- [22] D. Needham, R. S. Nunn, Biophys. J. 1990, 58, 997.
- [23] P. Wongtrakul, M. Abe, J. Manosroi, F. Sugawara, M. Yuasa, H. Sakai, A. Manosroi, *Colloids Surf.*, B 2003, 30, 129.
- [24] P. Balakrishnan, S. Shanmugam, W. S. Lee, W. M. Lee, J. O. Kim, D. H. Oh, D. D. Kim, J. S. Kim, B. K. Yoo, H. G. Choi, J. S. Woo, C. S. Yong, *Int. J. Pharm.* 2009, 377, 1.
- [25] M. Tabbakhian, N. Tavakoli, M. R. Jaafari, S. Daneshamouz, Int. J. Pharm. 2006, 323, 1.
- [26] A. Manosroi, R. Chutoprapat, M. Abe, J. Manosroi, Int. J. Pharm. 2008, 352, 248.
- [27] H. Abdelkader, U. Farghaly, H. Moharram, J. Pharm. Invest. 2014, 44, 329.
- [28] G. Puras, E. Fernández, G. Martínez-Navarrete, N. Attia, M. Mashal, J. L. Pedraz, J. Controlled Release 2017, 254, 55.

- [29] A. Kara, C. Rouillard, J. Mathault, M. Boisvert, F. Tessier, H. Landari, I. Melki, M. Laprise-Pelletier, E. Boisselier, M. A. Fortin, E. Boilard, J. Greener, A. Miled, Sensors 2016, 16, 778.
- [30] C. T. Lo, A. Jahn, L. E. Locascio, W. N. Vreeland, *Langmuir* 2010, 26, 8559.
- [31] F. Tessier, M. Laprise-Pelletier, E. Boilard, M. A. Fortin, A. Miled, in Annual Int. Conf. of the IEEE Engineering in Medicine and Biology Society (EMBS), Institute of Electrical and Electronics Engineers (IEEE), Orlando, FL, USA 2016, p. 2998.
- [32] N. M. Belliveau, J. Huft, P. J. Lin, S. Chen, A. K. Leung, T. J. Leaver, A. W. Wild, J. B. Lee, R. J. Taylor, Y. K. Tam, C. L. Hansen, P. R. Cullis, Mol. Ther.—Nucleic Acids 2012, 1, e37.
- [33] Z. Luo, L. Jiang, C. Ding, B. Hu, X. J. Loh, Z. Li, Y. L. Wu, Adv. Healthcare Mater. 2018, 7, 1801221.
- [34] Y. Barenholz, J. Controlled Release 2012, 160, 117.
- [35] P. P. Wibroe, D. Ahmadvand, M. A. Oghabian, A. Yaghmur, S. M. Moghimi, J. Controlled Release 2016, 221, 1.
- [36] C. Li, W. Guo, C. Wang, J. Cui, L. Zhang, Y. Wang, L. Zhang, Y. Li, Y. Hao, J. Controlled Release 2006, 118, 204.
- [37] M. J. Ernsting, M. Murakami, A. Roy, S.-D. Li, J. Controlled Release 2013, 172, 782.
- [38] G. T. Colbern, F. J. Martin, P. K. Working, M. A. Amantea, R. A. Hilger, D. M. Vail, Semin. Oncol. 2005, 31, 16.
- [39] A. Gabizon, D. Tzemach, L. Mak, M. Bronstein, A. T. Horowitz, J. Drug Targeting 2002, 10, 539.
- [40] T. Tagami, M. J. Ernsting, S. D. Li, J. Controlled Release 2011, 152, 303.
- [41] Z. Zhou, M. J. Xu, B. Gao, Cell Mol. Immunol. 2016, 13, 301.
- [42] H. Li, H. You, X. Fan, J. Jia, BMJ Open Gastroenterol. 2016, 3, e000079.
- [43] Y. Ohara, T. Oda, K. Yamada, S. Hashimoto, Y. Akashi, R. Miyamoto, A. Kobayashi, K. Fukunaga, R. Sasaki, N. Ohkohchi, *Int. J. Cancer* 2012, 131, 2402.
- [44] A. Ondo-Mendez, L. Del Riesgo, F. Castillo-Rivera, R. Garzón, F. Nualart, M. L. Pinzón-Daza, Y. Cuellar-Saenz, J. Cell. Biochem. 2017, 118, 1868.
- [45] J. Kreuter, D. Shamenkov, V. Petrov, P. Ramge, K. Cychutek, C. Koch-Brandt, R. Alyautdin, J. Drug Targeting 2002, 10, 317.
- [46] K. Prabhakar, S. M. Afzal, G. Surender, V. Kishan, Acta Pharm. Sin. B 2013, 3, 345.
- [47] M. S. Brown, J. L. Goldstein, J. Clin. Invest. 1983, 72, 743.
- [48] A. Akinc, W. Querbes, S. De, J. Qin, M. Frank-Kamenetsky, K. N. Jayaprakash, M. Jayaraman, K. G. Rajeev, W. L. Cantley, J. R. Dorkin, J. S. Butler, L. Qin, T. Racie, A. Sprague, E. Fava, A. Zeigerer, M. J. Hope, M. Zerial, D. W. Sah, K. Fitzgerald, M. A. Tracy, M. Manoharan, V. Koteliansky, A. De Fougerolles, M. A. Maier, Mol. Ther. 2010, 18, 1357.
- [49] J. A. Kulkarni, J. L. Myhre, S. Chen, Y. Y. C. Tam, A. Danescu, J. M. Richman, P. R. Cullis, *Nanomedicine* 2017, 13, 1377.
- [50] V. Kumar, J. Qin, Y. Jiang, R. G. Duncan, B. Brigham, S. Fishman, J. K. Nair, A. Akinc, S. A. Barros, P. V. Kasperkovitz, Mol. Ther.— Nucleic Acids 2014, 3, e210.

- [51] M. Tamaru, H. Akita, T. Nakatani, K. Kajimoto, Y. Sato, H. Hatakeyama, H. Harashima, Int. J. Nanomed. 2014, 9, 4267.
- [52] R. L. Rungta, H. B. Choi, P. J. C. Lin, R. W. Y. Ko, D. Ashby, J. Nair, M. Manoharan, P. R. Cullis, B. A. MacVicar, Mol. Ther.—Nucleic Acids 2013, 2, e136.
- [53] W. J. Schneider, J. Nimpf, Cell. Mol. Life Sci. 2003, 60, 892.
- [54] A. Tomak, H. M. Zareie, Y. Baran, V. Bulmus, I. Ozer, Biomacromolecules 2017, 18, 2699.
- [55] S. B. Gjedde, A. Gjeode, Comp. Biochem. Physiol., Part A: Physiol. 1980, 67, 671.
- [56] F. Braet, E. Wisse, Comp. Hepatol. 2002, 1, 1.
- [57] F. Porta, J. Huwyler, S. H. Schenk, D. Witzigmann, P. Grossen, K. Kiene, A. Ernst, Eur. J. Pharm. Biopharm. 2017, 119, 322.
- [58] U. Pieper-Fürst, F. Lammert, Biochim. Biophys. Acta 2013, 1831,
- [59] S. K. Asrani, H. Devarbhavi, J. Eaton, P. S. Kamath, J. Hepatol. 2019, 70, 151.
- [60] A. A. Mokdad, A. D. Lopez, S. Shahraz, R. Lozano, A. H. Mokdad, J. Stanaway, C. J. L. Murray, M. Naghavi, BMC Med. 2014, 12, 1.
- [61] R. Raphemot, D. Posfai, E. R. Derbyshire, J. Clin. Invest. 2016, 126, 2013
- [62] J. K. Tibenderana, U. D'Alessandro, A. Erhart, P. J. Rosenthal, J. Achan, A. Yeka, F. N. Baliraine, A. O. Talisuna, *Malar. J.* 2011, 10, 144
- [63] M. Oliver, F. Simon, F. de Monbrison, A. H. Beavogui, B. Pradines, C. Ragot, J. L. Moalic, C. Rapp, S. Picot, Med. Maladies Infect. 2008, 38, 169.
- [64] L. S. Wang, L. S. D'Souza, I. M. Jacobson, J. Med. Virol. 2016, 88, 1844.
- [65] L. A. J. O'Neill, E. J. Hennessy, A. E. Parker, Nat. Rev. Drug Discovery 2010, 9, 293
- [66] M. A. Tomai, R. L. Miller, K. E. Lipson, W. C. Kieper, I. E. Zarraga, J. P. Vasilakos, Expert Rev. Vaccines 2007, 6, 835.
- [67] M. H. Farzaei, M. Zobeiri, F. Parvizi, F. F. El-Senduny, I. Marmouzi, E. Coy-Barrera, R. Naseri, S. M. Nabavi, R. Rahimi, M. Abdollahi, Nutrients 2018, 10, 855.
- [68] M. Mehanny, R. M. Hathout, A. S. Geneidi, S. Mansour, J. Controlled Release 2016, 225, 1.
- [69] J. F. Mukerabigwi, X. Huang, W. Xiao, Y. Cao, S. Wang, S. Luo, X. Xie, J. Mei, Y. Zhang, RSC Adv. 2016, 6, 31607.
- [70] J. A. Kulkarni, M. M. Darjuan, J. E. Mercer, S. Chen, R. Van Der Meel, J. L. Thewalt, Y. Y. C. Tam, P. R. Cullis, ACS Nano 2018, 12, 4787
- [71] A. Yavlovich, A. Singh, R. Blumenthal, A. Puri, Biochim. Biophys. Acta, Biomembr. 2011, 1808, 117.
- [72] Y. Zhang, M. Huo, J. Zhou, S. Xie, Comput. Methods Programs Biomed. 2010, 99, 306.
- [73] A. Dagan, S. Gatt, S. Cerbu-Karabat, J.-C. Maziere, C. Maziere, R. Santus, E. L. Engelhardt, K. A. Yeh, C. C. Stobbe, M. C. Fenning, J. D. Chapman, *Int. J. Cancer* 1995, 63, 831.